PAPER • OPEN ACCESS

Enhanced generation of angle correlated photon-pairs in nonlinear metasurfaces

New Journal of Physics
The open access journal at the forefront of physics

Deutsche Physikalische Gesellschaft DPG
IOP Institute of Physics

Published in partnership with: Deutsche Physikalische Gesellschaft and the Institute of Physics

OPEN ACCESS

RECEIVED
20 November 2021

REVISED
11 February 2022

ACCEPTED FOR PUBLICATION
1 March 2022

PUBLISHED
24 March 2022

PAPER

Enhanced generation of angle correlated photon-pairs in nonlinear metasurfaces

Andrea Mazzanti[1,2], Matthew Parry[2,3], Alexander N Poddubny[2,4,5], Giuseppe Della Valle[1,6], Dragomir N Neshev[2,3] and Andrey A Sukhorukov[2,3*]

[1] Department of Physics, Politecnico di Milano, Piazza Leonardo da Vinci 32, I-20133, Milano, Italy
[2] Research School of Physics, Australian National University, Canberra, ACT 2601, Australia
[3] ARC Centre of Excellence for Transformative Meta-Optical Systems (TMOS), Australia
[4] ITMO University, 49 Kronverksky Pr., Saint Petersburg 197101, Russia
[5] Ioffe Physical Technical Institute, 26 Politekhnicheskaya, 194021, St Petersburg, Russia
[6] Istituto di Fotonica e Nanotecnologie, Consiglio Nazionale delle Ricerche, Milan, Italy
[*] Author to whom any correspondence should be addressed.

E-mail: andrea.mazzanti@polimi.it and andrey.sukhorukov@anu.edu.au

Keywords: nonlinear metasurface, entangled photons, quantum correlations, bound state in the continuum, spontaneous parametric downconversion

Abstract

We reveal that strongly enhanced generation of photon pairs with narrow frequency spectra and sharp angular correlations can be realised through spontaneous parametric down-conversion in metasurfaces. This is facilitated by creating meta-gratings through nano-structuring of nonlinear films of sub-wavelength thickness to support the extended bound state in the continuum resonances, associated with ultra-high Q-factors, at the biphoton wavelengths across a wide range of emission angles. Such spectral features of photons can be beneficial for various applications, including quantum imaging. Our modelling demonstrates a pronounced enhancement, compared to unpatterned films, of the total photon-pair generation rate normalized to the pump power reaching 1.75 kHz mW^{-1}, which is robust with respect to the angular bandwidth of the pump, supporting the feasibility of future experimental realisations.

1. Introduction

Metasurfaces, periodic sub-wavelength arrangements of nanoresonators, have brought forth significant advances in photonics. By tailoring the geometry and permittivity of the constitutive scattering elements, known as meta-atoms, advanced optical functionalities have been realized (see e.g. [1–6] and references therein). In particular, all-dielectric metasurfaces have been demonstrated to exhibit enhanced nonlinear optical responses due to the exploitation of Mie resonances in the meta-atoms and the subsequent high field enhancement at the nanoscale [7–11].

The increased nonlinear efficiency in resonant nanostructures can also facilitate the development of quantum sources based on spontaneous frequency mixing, such as spontaneous parametric down-conversion (SPDC) in media with quadratic nonlinearity [12, 13]. Indeed, miniaturization of photon-pair sources below the micron scale is particularly sought after, because of the possibility of working in the absence of the longitudinal phase matching condition, especially in configurations operated at room temperature [14–17]. A sub-micron photon-pair source exploiting the excitation of Mie resonances in isolated cylindrical nanoantennas has been demonstrated [18]. Recently, a resonant enhancement of photon-pair generation in metasurfaces was observed [19]. These first demonstrations prove the applicability of metasurfaces as quantum photon sources, however the relatively low Q-factor of the employed Mie resonances motivates research towards further enhancement of photon-pair rates, as well as tailoring of the quantum correlations.

Notably, the strongest enhancement of nonlinear interactions in metasurfaces can be achieved through resonances based on bound states in the continuum (BICs) [20–22]. It was recently suggested theoretically

that BICs in metasurfaces composed of reduced-symmetry nanoresonators can be used to enhance the photon-pair generation rate and spectral brightness [23]. However, the photon emission was predicted to occur primarily in the close to normal direction. It remained an outstanding question how to facilitate BIC-enhanced photon-pair emission over a large range of angles, which can lead to new opportunities for quantum imaging [24] based on angle-correlated photons.

Among the plethora of metasurface configurations so far reported in the literature, 1D meta-gratings in the form of sub-wavelength arrays of resonant nanowires have been recently thoroughly investigated [25]. It was suggested that arrays of silver nanostripes can enhance generation and emission in the normal direction of photon pairs [26], however plasmonic losses may detrimentally affect the quantum fidelity and we therefore consider all-dielectric structures. Although there are fewer design degrees of freedom compared to 2D patterns, 1D structures can sustain highly tunable BICs both at and off the Γ-point of the first Brillouin zone [27, 28]. The simpler design also results in fewer restrictions during the fabrication process, thus leading to a clear-cut observation of high Q-factor resonances associated with BICs [29] and enhanced second-harmonic generation [30].

The paper is organised as following. In section 2, we report on the theoretical design of a 1D nonlinear metasurface, based on AlGaAs material with strong quadratic nonlinearity, which supports off Γ BIC resonances in the telecom range. We demonstrate in section 3 that the high field enhancement achieved at the fundamental frequency leads to second-order nonlinear optical processes with efficiencies several orders of magnitude higher than both the unpatterned film and the Mie resonant metastructure configurations. Through a combination of finite element methods (FEM) and semi-analytical modeling of the BIC dispersion, we calculate the photon-pair generation rate. We predict that the high contrast in field enhancement at resonance results in an extremely narrow angular and temporal bandwidth for the emitted photon-pairs, accordingly implying their sharp angular correlations. Finally, we demonstrate that the total SPDC efficiency, integrated over all angles and frequencies, is weakly dependent on the angular bandwidth of the pump beam, demonstrating the experimental feasibility of the proposed system. We present conclusions in section 4.

2. Meta-grating with photon-pair bound states in the continuum

Our design consists of a periodic arrangement of filleted nanowires, or *nanofins*, as presented in figure 1(a). The pump photon (green arrow) is impinging from the substrate side, and consequently a signal (orange arrow) and an idler (blue arrow) photons are emitted in the forward direction (on the air side), conserving transverse momentum and energy of the pump photon, as sketched in figure 1(b). This implies strong angular correlations between the signal and idler photons, since they are emitted with the opposite transverse momenta components.

Whereas our concept can be applied to different quadratically nonlinear materials, in numerical simulation we consider the nanofins made of (110)-cut $Al_{0.18}Ga_{0.82}As$, positioned on a dielectric substrate ($\varepsilon_{sub} = 2$). AlGaAs poses an enticing alternative to GaAs, as it is possible to blue-shift the material band gap by increasing the aluminum fraction of the semiconductor [31], which enables us to operate in a wavelength range which was previously inaccessible. In particular, an aluminum fraction of 0.18 leads to a band gap of $E_g = 1.65$ eV (corresponding to $\lambda_g = 751$ nm) [32]. Accordingly, this can facilitate the photon-pair generation in the telecommunication band with the wavelengths ∼1500 nm.

Our idea for the SPDC enhancement is to exploit the left/right symmetry of the metasurface so as to simultaneously support two degenerate BICs for the generated photons emitted at opposite angles. To design the structure, we choose a sub-wavelength periodicity of $D = 530$ nm, which ensures that no diffraction orders are present at either the photon-pair fundamental frequency (∼1500 nm) or at the sum-frequency pump wavelength (∼750 nm). By doing so, we avoid the SPDC generation in unwanted radiation channels, which could otherwise lead to a lower quantum state fidelity.

We aim to employ the 'non-accidental' BIC resonances, where slight variations in the geometry would lead to a detuning of the BICs present in the structure, with no detrimental effect on the overall efficiency [27]. The resonant frequency matching for the photon-pairs is a key design aspect, which can be satisfied by tuning the structure geometry. Additionally, there are other aspects to be considered in the design, namely: the field enhancement pattern should be peaked inside of the nanofin, for maximum conversion efficiency; the direction of emission should be angled, so to allow for signal and idler to be emitted at different optical paths; the BIC mode should have a non-zero overlap with a propagating mode (e.g. a plane wave or a Gaussian beam), to successfully couple to a radiative channel.

We performed eigenfrequency studies of the structure based on FEM simulations with COMSOL Multiphysics 5.6, and tuned the geometry to satisfy the requirements formulated above. The search for quasi-BIC modes was performed by eigenfrequency analysis of the configuration of figure 1(a), using

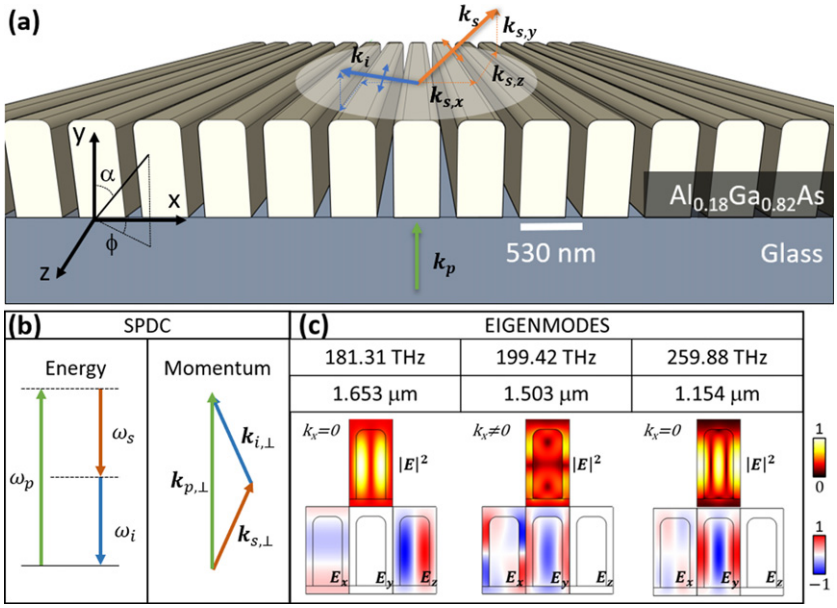

Figure 1. (a) Proposed design of the metasurface, in the form of meta-grating composed of nanofins. The scale bar corresponds to the metasurface periodicity $D = 530$ nm. Thick double pointed arrows that are transverse to the $\mathbf{k}_{s,i}$ wavevectors shown above the metasurface indicate the *p*-polarization of the signal and idler electric field corresponding to off-normal resonance. (b) Sketch of energy and transverse (*x*, *z* components) momentum conservation in the SPDC process: a pump photon (green) is absorbed by the active material and a pair of lower energy photons is emitted, a signal (orange) and an idler (blue) photon. (c) Normalized field enhancement and field components patterns in correspondence of three different quasi-BIC resonances, sustained by the nanofins metasurface at $k_z = 0$.

Floquet periodic boundary conditions (BCs) on the lateral boundaries (parallel to the *y* axis), and perfectly matched layers (PMLs) on the upper (air side) and lower (substrate side) domains. We took into account the translational invariance of the metasurface geometry along the *z*-direction, while the period along the *x*-direction has been tailored to forbid emission in the higher-order diffracted orders both at the fundamental and sum-frequency wavelengths. We then ran multiple simulations sweeping over k_x and k_z, corresponding to different polar and azimuthal angles of incidence (α, ϕ) as sketched in figure 1(a), and identified the frequency and linewidth of the quasi-BIC resonances associated with the highest *Q*-factor values.

We find the optimal nanofins dimensions with a lateral width of $w = 360$ nm and a height of $H = 850$ nm. In order to avoid unphysical field distribution at the sharp-edges, we smoothed the top edges of the nanofins with a fillet radius $R_f = 100$ nm. It is worth noting that by considering a supported configuration with a substrate and a rounded profile for the top edges of the nanofins, we account for the realistic experimental conditions at the cost of eliminating the up/down inversion symmetry of the metasurface with respect to the *z*-axis. The symmetry breaking results in radiation losses of the BIC, which then becomes a quasi-BIC [33, 34]. Most importantly, these resonances are robust with respect to a specific geometry of the top edges, provided that the array periodicity is accurately satisfied, which is within the standard capabilities of modern top–down nanofabrication technology.

We identify several BIC resonances in the infrared spectral region, and show their field profiles in figure 1(c). We find that the most suitable for nonlinear enhancement at the off Γ BIC is at $\nu_{BIC} = 199.42$ THz ($\lambda_{BIC} = 1503.35$ nm). This particular resonance is well-coupled to a *p*-polarized plane wave (since the *z*-component of the electric field is null), at a propagation polar angle of $\alpha \approx 23°$, and the field enhancement pattern is mostly uniform inside the resonator. For comparison, there appear two other BICs at normal incidence with much higher *Q*-factors than the off-normal BIC, since the latter resonances are not affected by the top–down symmetry breaking. Specifically, the one at 181 THz has an odd symmetry of the in-plane electric field component E_z, while the one at 259 THz has most of the electrical field along the *y* axis, which is the direction normal to the metasurface. Since our aim is the generation of angle-correlated photons, only the off-normal BIC is suitable, and we analyze the associated *p*-polarized photon emission in the following. It is worth noting that this kind of quasi-BIC can be easily tuned by adjusting the geometrical parameters. In particular, for a fixed ratio between the width of the nanofin and the air gap, an increase of the array periodicity results in a redshift of the quasi-BIC and a smaller emission angle of BIC resonance [35].

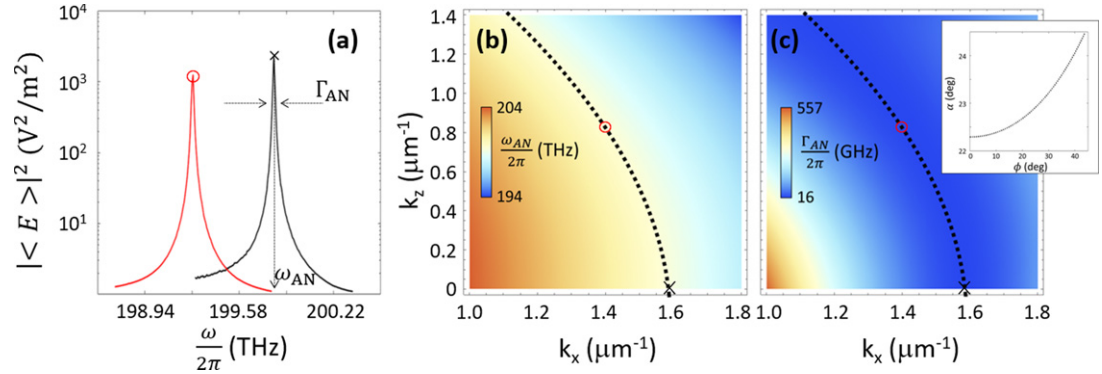

Figure 2. (a) Simulated modulus squared of the average electric field inside the nanofin in correspondence of two different incidence angles for the driving plane wave. Black arrows indicate the FWHM of the feature and the central angular frequency. (b) and (c) Analytical approximation of (b) resonant frequency and (c) linewidth of the field enhancement inside of the nanofin as a function of the in-plane wave vector. The quasi-BIC position is marked by a dashed black curve in both panels. The red circle and black cross represent the excitation conditions for the red and black curves in panel (a), respectively. Inset shows the α and ϕ angles for which the resonance has minimum linewidth, corresponding to the dashed line in k-space shown in panel (c).

3. Enhanced photon-pair generation

We study the photon-pair generation and quantify the enhancement due to BIC resonances by employing the general theoretical methodology formulated in references [13, 18, 23], which was previously applied to nanoresonators and 2D metasurfaces.

We begin our study by obtaining an analytical approximation of the BIC dispersion relations in the metasurface. We ran an ensemble of linear simulations for the p-polarized signal beam, scanning the plane wave frequency, polar and azimuthal angles of incidence (α, ϕ) as sketched in figure 1(a). As characteristic examples, we show in figure 2(a) the square of the average electric field norm inside of each nanofin vs the frequency of a plane wave impinging at $\alpha = 22.5^\circ$ and $\phi = 0^\circ$ (black trace), and at $\alpha = 23.5^\circ$ and $\phi = 30^\circ$ (red trace). Note that, even considering the presence of a substrate in our model, both of these features are particularly narrow, corresponding to a Q-factor of approximately 3.5×10^4. We find that, at the BIC resonance, the resulting electric field modulus squared is well approximated by a Lorentzian function [36] defined as:

$$L(\omega, k_x, k_z) = \frac{1}{\pi} \frac{\frac{1}{2}\Gamma_{\mathrm{AN}}(k_x, k_z)}{\left[\frac{1}{2}\Gamma_{\mathrm{AN}}(k_x, k_z)\right]^2 + [\omega - \omega_{\mathrm{AN}}(k_x, k_z)]^2}, \tag{1}$$

where $\omega_{\mathrm{AN}}(k_x, k_z)$ is the peak position and $\Gamma_{\mathrm{AN}}(k_x, k_z)$ is the full width at half maximum (FWHM) of the resonance.

Based on the results gathered by FEM calculations, we find an accurate analytical fitting for the dispersion of peak position and FWHM as follows:

$$\begin{aligned} \Gamma_{\mathrm{AN}}(k_{s,x}, k_{s,z}) &= a(k_{s,z})[k_{s,x} - k_{s,x}^{\mathrm{BIC}}(k_{s,z})]^2 + \Gamma_0, \\ \omega_{\mathrm{AN}}(k_{s,x}, k_{s,z}) &= b[k_{s,x} - k_{s,x}^{\mathrm{BIC}}(k_{s,z})] + \overline{\omega}_0, \end{aligned} \tag{2}$$

where $\overline{\omega}_0 = 2\pi\nu_{\mathrm{BIC}}$ is the angular frequency of the quasi-BIC, $\Gamma_0 = 2\pi$ 16 GHz is the minimum FWHM of the resonance, and $k_{s,x}^{\mathrm{BIC}}(k_{s,z}) = -0.36\ \mu m\, k_{s,z}^2 + 1.6\ \mu m^{-1}$ is the function that describes the position of the BIC in k_s-space. Lastly, we determined the fitting parameters $a = -8.2 \times 10^{-6}$ Hz m$^3|k_{s,z}| + 11.5812$ Hz m^2 and $b = -52$ MHz m.

We show the dependencies of the resonance linewidth and frequency, calculated using equation (2), on the transverse wavevector components of a signal photon in figures 2(b) and (c). Note that the quasi-BIC exhibits a parabolic dispersion in the k_s-space (dashed black curve). Along this parabola in the reciprocal space, the peak frequency is roughly constant ($\nu_{\mathrm{BIC}} = \overline{\omega}_0/(2\pi)$) and the linewidth is equal to Γ_0, showing that the wavelength and Q-factor are weakly dependent on the angle of emission of the quasi-BIC. These features are satisfied in the considered transverse wavevector domain where the polar angle α remains close to 23.5° as shown in the inset of figure 2(c). The resonance broadens and ceases to exist when k_x is reduced further, and we do not consider this regime in the following.

With the dispersion of the BIC resonance at hand, we perform a quantitative estimation of the quantum photon-pair rate generated through SPDC by employing the quantum–classical correspondence with the inverse process of SPDC: that is, sum-frequency generation (SFG) [12, 13, 37]. We thus considered two plane waves (the signal and the idler) impinging from air, that generate a SFG signal (corresponding to the

pump in the SPDC process) propagating in the substrate (which is the opposite direction of the process sketched in figure 1(a)) and numerically evaluated the efficiency of this process, referred to as η_{SFG}. This is defined as the ratio between the intensity of the SFG signal and the product of the signal and idler incident intensities, i.e. $\eta_{\mathrm{SFG}} = I_{\mathrm{SFG}}/I_{\mathrm{s}}I_{\mathrm{i}}$. Then the quantum photon-pair rate of the SPDC process is retrieved according to the equations:

$$\frac{\mathrm{d}N_{\mathrm{pair}}}{\mathrm{d}t} = \frac{\lambda_{\mathrm{p}}^2}{(2\pi)^3\lambda_{\mathrm{s}}\lambda_{\mathrm{i}}}P_{\mathrm{p}}\eta_{\mathrm{SPDC}}, \tag{3}$$

$$\eta_{\mathrm{SPDC}} = \iiint \eta_{\mathrm{SFG}}(\omega_{\mathrm{s}}, \boldsymbol{k}_{\mathrm{s},\perp})\mathrm{d}\omega_{\mathrm{s}}\,\mathrm{d}\boldsymbol{k}_{\mathrm{s},\perp}, \tag{4}$$

where N_{pair} is the number of generated photon pairs, P_{p} is the pump beam power, λ_{p}, λ_{s}, and λ_{i} are the pump, signal, and idler wavelengths respectively, $\omega_{\mathrm{s}} = 2\pi c/\lambda_{\mathrm{s}}$ is the signal angular frequency, and $\boldsymbol{k}_{\mathbf{s},\perp}$ is the projection of the signal wave vector on the metasurface plane (x, z). Because the BIC exists for a broad range of transverse wavenumbers, the result in equation (3) depends on the integration limits ω and k_{s}-space. In the following, we limit the integration to the reciprocal space represented in figure 2(b), corresponding to a numerical aperture NA ~ 0.34. Such a choice represent characteristic experimental conditions.

We determine the SFG efficiency by simulating the nonlinear response of the metasurface under symmetric illumination with two (signal and idler) p-polarized plane waves, such that the in-plane wavevectors are opposite ($\boldsymbol{k}_{\mathrm{s},\perp} = -\boldsymbol{k}_{\mathrm{i},\perp}$), which satisfies transverse momentum conservation with the sum-frequency wave that propagates normally with respect to the metasurface. We consider the signal and idler waves impinging from the air-side at angles α around $\pm 23^{\circ}$, in a range of frequencies close to the quasi-BIC. According to the quantum–classical correspondence, we need to analyse the SFG in the regime of low conversion efficiency, when the signal and idler dynamics is linear. Accordingly, we perform numerical FEM analysis by defining two independent linear studies, which determine the total electromagnetic field in the structure for the signal and idler beams, with Floquet BCs on the sides and ports excitation conditions on the above and below. The resulting fields inside of the nanofins are used to calculate the nonlinear polarization defined through the quadratic susceptibility tensor, which drives the time-harmonic Maxwell equations at the SFG frequency. For this last step, the port conditions are replaced by PMLs backed by scattering BCs, and the SFG intensity is retrieved as the projection of the calculated field onto the plane wave basis that describes the transmitted spatial spectrum after the metasurface, as detailed in [38]. However, because of the sub-wavelength periodicity, there is only one output sum-frequency plane wave in the forward direction, i.e. emitted on the substrate side, with a purely real $\boldsymbol{k}$ vector.

Importantly, the orientation of the crystallographic axes plays an important role in defining the total throughput of the SFG process [23, 39]. Indeed, the most appropriate crystal cut would lead to a higher nonlinear current in the material, as well as a better overlap between the nonlinear polarization mode and the radiating SFG pattern. As an example, we present the nonlinear polarization vector norm in the case of a (111)-cut crystal (figure 3(a)) and (110)-cut crystal (figure 3(b)). In the latter, we consider an additional rotation of the crystal axes by $\pi/4$ around the y-axis, since this proved to be the configuration with the best performances. Note that although the spatial patterns are similar, the intensity is much higher, by around a factor of three, in the (110)-cut case. The higher nonlinear drive results in a three orders of magnitude higher SFG efficiency when both signal and idler are at the resonant condition, as shown in figure 3(c). Furthermore, the forward (black) and backward (red) efficiencies for a (110)-cut (solid traces) and (111)-cut (dashed traces) show that the (110)-cut configuration is more efficient in radiating SFG in the forward direction, as opposed to the (111)-cut. We further analyze the most efficient case of (110)-cut, and find that the SFG radiation has negligible z component of the electric field. We therefore consider the p-polarized pump for the SPDC process in the following.

For comparison, we also compute the SFG efficiency from an unstructured film of AlGaAs (dotted traces) with the same thickness as the nanofin metasurfaces, which turned out to be in the range of 10^{-22}–10^{-21} m^2 W^{-1}. This highlights the much higher nonlinear efficiency introduced by the nanostructuring, despite of the removal of part of the nonlinear medium, when exploiting resonant metasurfaces. Moreover, note that the typical value achievable with Mie resonances is $\sim 10^{-17}$ m^2 W^{-1} [18, 40], which is nevertheless from 3 to 6 orders of magnitude lower than in the 1D metasurfaces with extended BICs, considered in our design.

To confirm the origin of SFG enhancement, we show in figure 3(d) the ratio between the SFG efficiency and the product of the squared moduli of the signal and idler electric fields for the (110)-cut metasurface. Note that this ratio is weakly dependent on the signal beam frequency. Indeed in the same frequency range for which the SFG intensity changes by three orders of magnitude (figure 3(c), solid black curve), this figure

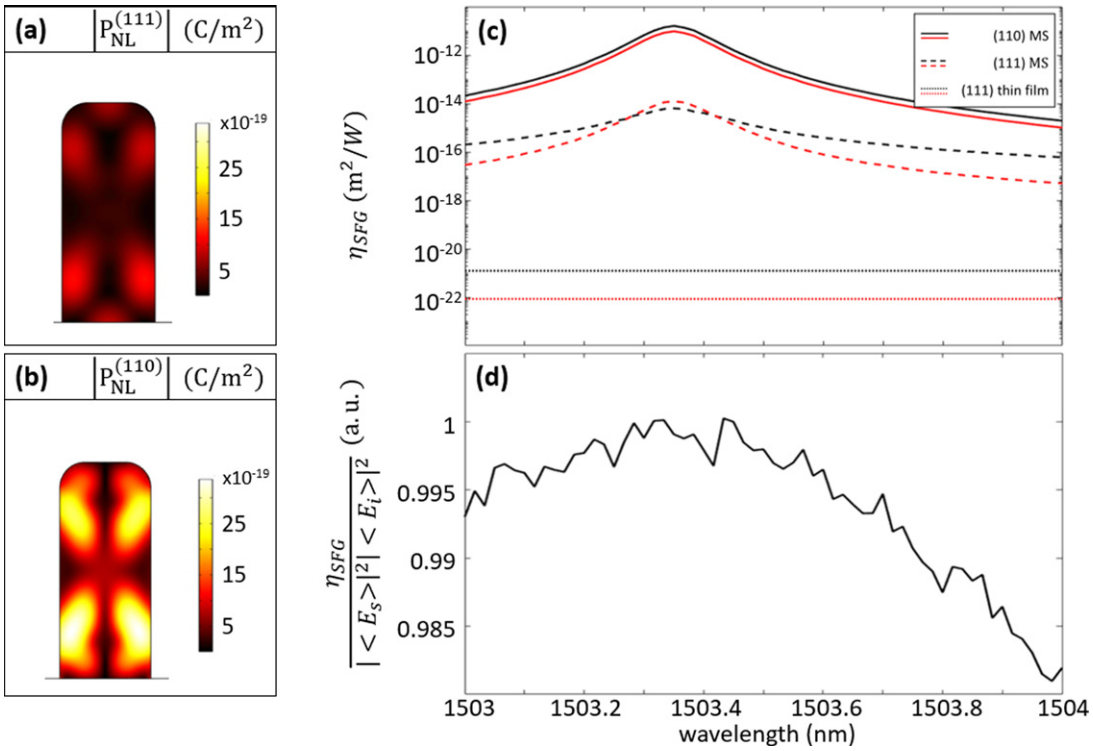

Figure 3. (a) and (b) Nonlinear polarization vector norm at the sum-frequency wavelength inside of the nanofin, in the case of (a) (111)-cut or (b) (110)-cut AlGaAs crystal. (c) Logarithmic plot of the SFG efficiency (in $m^2\ W^{-1}$), emitted in the forward (black) or backward (red) direction, as a function the signal frequency in the case of a thin film of AlGaAs (dotted) a (111)-cut metasurface (dashed) or (110)-cut metasurface with an additional rotation of $\pi/4$ with respect to the y-axis (solid). (d) SFG efficiency in the forward direction for the (110)-cut metasurface, divided by the product of the moduli squared of the average field enhancement norm inside the resonator for signal and idler.

of merit is relatively constant. Therefore, we conclude that the SFG efficiency linearly scales with the product of signal and idler electric fields modulus squared, i.e. $\eta_{\mathrm{SFG}} \propto |\boldsymbol{E}_{\mathrm{s}}|^2|\boldsymbol{E}_{\mathrm{i}}|^2$. We also performed simulations at different incident angles of the signal and idler, and found agreement with this relationship. Accordingly, using the analytical expression for the field enhancement and considering that in the SPDC process energy and transverse momentum have to be conserved, the SFG efficiency can be evaluated as:

$$\eta_{\mathrm{SFG}}(\omega_{\mathrm{s}}, \boldsymbol{k}_{\mathrm{s},\perp}; \omega_{\mathrm{p}}, \boldsymbol{k}_{\mathrm{p},\perp}) = \eta_0 L(\omega_{\mathrm{s}}, \boldsymbol{k}_{\mathrm{s},\perp}) L(\omega_{\mathrm{p}} - \omega_{\mathrm{s}}, \boldsymbol{k}_{\mathrm{p},\perp} - \boldsymbol{k}_{\mathrm{s},\perp}), \tag{5}$$

where ω_{p}, ω_{s}, $\boldsymbol{k}_{\mathrm{p},\perp}$, $\boldsymbol{k}_{\mathrm{s},\perp}$ are the angular frequency and parallel wave vector (i.e. belonging to the x, z-plane) of the pump and signal photon respectively, and $\eta_0 = 3.617\,98 \times 10^{10}\ \mathrm{m^2\ s^2\ W^{-1}}$ is a constant factor, extrapolated from FEM analysis.

We can estimate the narrowness of the emission angular spectrum for the SPDC process by calculating η_ω, defined as the integral over ω_{s} of the SFG efficiency. Interestingly, it can be expressed analytically as follows:

$$\begin{aligned}\eta_\omega(\boldsymbol{k}_{\mathrm{s},\perp}; \omega_{\mathrm{p}}, \boldsymbol{k}_{\mathrm{p},\perp}) &= \int_{-\infty}^{+\infty} \eta_{\mathrm{SFG}}(\omega_{\mathrm{s}}, \boldsymbol{k}_{\mathrm{s},\perp}; \omega_{\mathrm{p}}, \boldsymbol{k}_{\mathrm{p},\perp}) \mathrm{d}\omega_{\mathrm{s}} \\ &= \frac{\eta_0}{\pi} \frac{\left[\frac{1}{2}\Gamma_{\mathrm{AN}}^{(\mathrm{s})} + \frac{1}{2}\Gamma_{\mathrm{AN}}^{(\mathrm{i})}\right]}{\left[\frac{1}{2}\Gamma_{\mathrm{AN}}^{(\mathrm{s})} + \frac{1}{2}\Gamma_{\mathrm{AN}}^{(\mathrm{i})}\right]^2 + \left[\omega_{\mathrm{p}} - (\omega_{\mathrm{AN}}^{(\mathrm{s})} + \omega_{\mathrm{AN}}^{(\mathrm{i})})\right]^2},\end{aligned}$$

where the superscripts (s) or (i) imply the evaluation of the analytically defined functions in equation (2) at the $\boldsymbol{k}_\perp$ of the signal or idler, respectively.

We anticipate the maximum SPDC enhancement when both the generated photons correspond to a BIC resonance. This can be achieved, in particular, in the degenerate configuration by exploiting the same BIC appearing at positive and negative emission angles. This case can be realised for the pump frequency $\omega_{\mathrm{p}} = 2\overline{\omega}_0$ at normal incidence, $\boldsymbol{k}_{\mathrm{p},\perp} = 0$. Indeed, under these assumptions, $\Gamma_{\mathrm{AN}}^{(\mathrm{s})} = \Gamma_{\mathrm{AN}}^{(\mathrm{i})}$ and $\omega_{\mathrm{AN}}^{(\mathrm{s})} = \omega_{\mathrm{AN}}^{(\mathrm{i})}$, corresponding to a maximum efficiency in equation (6). For a high Q-factor resonance, this lead to a very narrow angular emission as shown in figure 4(a). Note that emission is expected to be present only at k values corresponding to the quasi-BIC, indicated by the dashed line in figures 2(b) and (c) with the inset representing the associated emission angles, with a giant contrast with respect to the background. We

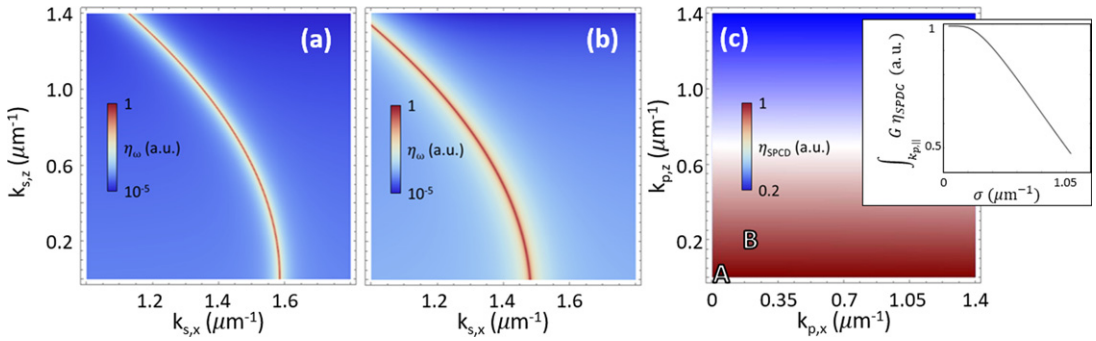

Figure 4. (a) and (b) Normalized SPDC efficiency, as a function of the signal wave vector, in the case of (a) pump beam at normal incidence or (b) slightly angled pump beam at $\alpha = 2^\circ$ and $\phi = 45^\circ$ corresponding to $k_{p,x} = k_{p,z} = 0.2\ \mu\text{m}^{-1}$. (c) Integrated SPDC efficiency as a function of the pump beam wave vector. Markers A and B represent the loci of the angle dependent efficiency represented in panels (a) and (b) respectively. The efficiency degradation is relatively low considering the large k values. Inset shows the angle integrated efficiency of SPDC as a function of the pump beam angular bandwidth, for a fixed total pump power.

checked that the peak SPDC efficiency values are fairly constant, with a relative variation below 10%, along the quasi-BIC line in the range of plotted wavenumbers in figure 4(a).

To better appreciate the narrowness of the emission pattern, in figure 4(b) we report η_ω in the case of off normal excitation. We observe that the symmetry breaking of the excitation condition has two main effects: (i) a shift of the emission pattern in the signal reciprocal space due to transverse momentum conservation and (ii) a noticeable broadening of the emission peak.

A fundamentally interesting question is what would happen to the total photon-pair rate if one realises a perfect BIC with an infinite Q-factor, corresponding to $\Gamma^{(s)}_{AN} = \Gamma^{(i)}_{AN} = 0$. Then, although the expression in equation (6) would diverge along the BIC parabola in momentum space, we find that its integral over k-space defining the overall SPDC efficiency according to equation (3) will be always finite. This suggests that a perfect BIC may not be required in practice, since similarly strong enhancement can be achieved based on quasi-BICs.

To further link our study to future experiments, we analyse the effect of the pump beam width on the SPDC process. The beam width is inversely proportional to the beam extent in the transverse momentum space. Accordingly, we analyse the SPDC efficiency dependence on $\boldsymbol{k}_{p,\perp}$. The integral in $\boldsymbol{k}_{s,\perp}$-space of $\eta_\omega(\boldsymbol{k}_{s,\perp}; \omega_p, \boldsymbol{k}_{p,\perp})|_{\omega_p = 2\overline{\omega}_0}$, which defines η_{SPDC}, does not possess a general analytical form. We calculated it semi-analytically, by determining numerically the poles of η_ω, and then making analytical evaluation of the integral via the residue theorem.

We show the total SPDC efficiency η_{SPDC} as a function of the pump transverse wavevector $\boldsymbol{k}_{p,\perp}$ in figure 4(c). Most remarkably, the efficiency reduction compared to the normal incidence is marginal, even for extremely large values of $|\boldsymbol{k}_{p,\perp}|$. Indeed, note that the two conditions shown in figures 4(a) and (b) correspond to relatively close loci in the η_{SPDC} map (markers A and B in figure 4(c)), and the total efficiently is roughly equal in both cases. Following these considerations our modeling proves that, once all of the contribution in the reciprocal space are considered, off-normal pump excitation does not impact on the overall efficiency of the SPDC process, yet it affects the angular width of the photon-pairs emission pattern.

The weak dependence demonstrated by η_{SPDC} with respect to $\boldsymbol{k}_{p,\perp}$ is advantageous when considering a practical pump beam with finite angular bandwidth. Indeed, we estimate that the degradation of the overall efficiency introduced by a pump angular profile described by a Gaussian distribution $G(k_{p,x}, k_{p,z}) = (2\pi\sigma)^{-1} \exp(-(k^2_{p,x} + k^2_{p,z})/2\sigma^2)$, is relatively negligible, approaching a factor of 0.5 in correspondence of a pump angular width of $\sigma \sim 1.05\ \mu\text{m}^{-1}$.

Finally, and most interestingly, when substituting η_{SPDC} in equation (3), we estimate a photon pair generation rate, normalized to the pump power, of 1.75 kHz mW^{-1}. This magnitude is similar to the prediction for BIC-enhanced in a 2D metasurface that emits in the normal direction [23], whereas the 1D metasurface considered in this work allows for a broad off-normal angular emission that may be desirable for different types of applications. We note that the aperture angle of signal or idler photon emission is relatively narrow, being about 8°, centred at 23° emission angle (i.e. from 19° to 27°), which can be efficiently captured with high-NA optics. On the other hand, the quantum source can provide wide-angle object illumination for quantum imaging with a single-photon sensitive camera.

4. Conclusions

In conclusion, we predicted that metasurfaces in the form of meta-gratings, created by periodic nanopatterning of a nonlinear film with sub-wavelength thickness, can facilitate strongly enhanced generation of photon-pairs through SPDC with a narrow spectrum across a broad range of emission angles. We presented a practical design based on AlGaAs material with strong quadratic nonlinearity, that provides the enhancement based on extended BIC resonances at the telecommunication wavelengths around the 1500 nm wavelength. We determined an accurate analytical approximation for the BIC dispersion and employed a rigorous quantum–classical correspondence to calculate the SPDC efficiency. We estimate the photon-pair generation rate of 1.75 kHz mW^{-1}, which is sustained under practical experimental conditions of a finite pump beam width. While the SPDC rate is similar to the maximum predicted enhancement in 2D metasurfaces with normal emission, the angular emission in our structures can offer new opportunities for diverse applications. Furthermore, we envisage a generalization of our design for the enhancement of angle-correlated and frequency non-degenerate photon-pair generation via a double-BIC metasurface configuration, which would be beneficial for quantum imaging. There is also an interesting possibility to realize resonant enhancement at the pump wavelength, allowing the use of less powerful pump lasers, which can benefit the integration in end-user devices.

Acknowledgments

We acknowledge the support by the Australian Research Council (Nos. DP190101559, CE200100010, and FT170100331). AM and GDV acknowledges the support of the European Union Horizon 2020 Research and Innovation Programme through the METAFAST Project (Grant No. 899673). The authors declare no conflicts of interest.

Data availability statement

The data that support the findings of this study are available upon reasonable request from the authors.

ORCID iDs

Matthew Parry https://orcid.org/0000-0002-1661-0810
Alexander N Poddubny https://orcid.org/0000-0002-4009-5070
Giuseppe Della Valle https://orcid.org/0000-0003-0117-2683
Dragomir N Neshev https://orcid.org/0000-0002-4508-8646
Andrey A Sukhorukov https://orcid.org/0000-0002-5116-5425

References

[1] Kildishev A V, Boltasseva A and Shalaev V M 2013 Planar photonics with metasurfaces *Science* **339** 1232009
[2] Yu N and Capasso F 2014 Flat optics with designer metasurfaces *Nat. Mater.* **13** 139–50
[3] Hsiao H-H, Chu C H and Tsai D P 2017 Fundamentals and applications of metasurfaces *Small Methods* **1** 1600064
[4] Neshev D and Aharonovich I 2018 Optical metasurfaces: new generation building blocks for multi-functional optics *Light: Sci. Appl.* **7** 58
[5] De Angelis C, Leo G and Neshev D N (ed) 2020 *Nonlinear Meta-Optics* (Boca Raton, FL: CRC Press)
[6] Solntsev A S, Agarwal G S and Kivshar Y S 2021 Metasurfaces for quantum photonics *Nat. Photon.* **15** 327–36
[7] Shcherbakov M R *et al* 2017 Ultrafast all-optical tuning of direct-gap semiconductor metasurfaces *Nat. Commun.* **8** 17
[8] Della Valle G *et al* 2017 Nonlinear anisotropic dielectric metasurfaces for ultrafast nanophotonics *ACS Photonics* **4** 2129–36
[9] Liu S, Vabishchevich P P, Vaskin A, Reno J L, Keeler G A, Sinclair M B, Staude I and Brener I 2018 An all-dielectric metasurface as a broadband optical frequency mixer *Nat. Commun.* **9** 2507
[10] Krasnok A, Tymchenko M and Alù A 2018 Nonlinear metasurfaces: a paradigm shift in nonlinear optics *Mater. Today* **21** 8–21
[11] Carletti L, Li C, Sautter J, Staude I, De Angelis C, Li T and Neshev D N 2019 Second harmonic generation in monolithic lithium niobate metasurfaces *Opt. Express* **27** 33390–7
[12] Poddubny A N, Iorsh I V and Sukhorukov A A 2016 Generation of photon-plasmon quantum states in nonlinear hyperbolic metamaterials *Phys. Rev. Lett.* **117** 123901
[13] Poddubny A N, Neshev D N and Sukhorukov A A 2020 Quantum nonlinear metasurfaces *Nonlinear Meta-Optics* ed C De Angelis, G Leo and D N Neshev (Boca Raton, FL: CRC Press) pp 147–80
[14] Okoth C, Cavanna A, Santiago-Cruz T and Chekhova M V 2019 Microscale generation of entangled photons without momentum conservation *Phys. Rev. Lett.* **123** 263602
[15] Okoth C, Kovlakov E, Bonsel F, Cavanna A, Straupe S, Kulik S P and Chekhova M V 2020 Idealized Einstein–Podolsky–Rosen states from non-phase-matched parametric down-conversion *Phys. Rev.* A **101** 011801(R)
[16] Santiago-Cruz T, Sultanov V, Zhang H, Krivitsky L A and Chekhova M V 2021 Entangled photons from subwavelength nonlinear films *Opt. Lett.* **46** 653–6

[17] Duong N M H et al 2021 Broadband photon pair generation from a single lithium niobate microcube (arXiv:2109.08489)
[18] Marino G et al 2019 Spontaneous photon-pair generation from a dielectric nanoantenna Optica 6 1416–22
[19] Santiago-Cruz T et al 2021 Photon pairs from resonant metasurfaces Nano Lett. 21 4423–9
[20] Hsu C W, Zhen B, Stone A D, Joannopoulos J D and Soljačić M 2016 Bound states in the continuum Nat. Rev. Mater. 1 16048
[21] Carletti L, Koshelev K, De Angelis C and Kivshar Y 2018 Giant nonlinear response at the nanoscale driven by bound states in the continuum Phys. Rev. Lett. 121 033903
[22] Koshelev K, Kruk S, Melik-Gaykazyan E, Choi J-H, Bogdanov A, Park H-G and Kivshar Y 2020 Subwavelength dielectric resonators for nonlinear nanophotonics Science 367 288–92
[23] Parry M, Mazzanti A, Poddubny A, Della Valle G, Neshev D N and Sukhorukov A A 2021 Enhanced generation of nondegenerate photon pairs in nonlinear metasurfaces Adv. Photon. 3 055001
[24] Moreau P-A, Toninelli E, Gregory T and Padgett M J 2019 Imaging with quantum states of light Nat. Rev. Phys. 1 367–80
[25] Lawrence M, Barton D R, Dixon J, Song J-H, van de Groep J, Brongersma M L and Dionne J A 2020 High quality factor phase gradient metasurfaces Nat. Nanotechnol. 15 956–61
[26] Jin B, Mishra D and Argyropoulos C 2021 Efficient single-photon pair generation by spontaneous parametric down-conversion in nonlinear plasmonic metasurfaces Nanoscale 13 19903–14
[27] Zhen B, Hsu C W, Lu L, Stone A D and Soljačić M 2014 Topological nature of optical bound states in the continuum Phys. Rev. Lett. 113 257401
[28] Ovcharenko A I, Blanchard C, Hugonin J-P and Sauvan C 2020 Bound states in the continuum in symmetric and asymmetric photonic crystal slabs Phys. Rev. B 101 155303
[29] Doeleman H M, Monticone F, den Hollander W, Alù A and Koenderink A F 2018 Experimental observation of a polarization vortex at an optical bound state in the continuum Nat. Photon. 12 397–401
[30] Huang Z et al 2021 Highly efficient second harmonic generation of thin film lithium niobate nanograting near bound states in the continuum Nanotechnology 32 325207
[31] Gili V F et al 2016 Monolithic AlGaAs second-harmonic nanoantennas Opt. Express 24 15965–71
[32] Adachi S 1994 GaAs and Related Materials: Bulk Semiconducting and Superlattice Properties (Singapore: World Scientific)
[33] Sadrieva Z F, Sinev I S, Koshelev K L, Samusev A, Iorsh I V, Takayama O, Malureanu R, Bogdanov A A and Lavrinenko A V 2017 Transition from optical bound states in the continuum to leaky resonances: role of substrate and roughness ACS Photonics 4 723–7
[34] Koshelev K, Lepeshov S, Liu M, Bogdanov A and Kivshar Y 2018 Asymmetric metasurfaces with high-Q resonances governed by bound states in the continuum Phys. Rev. Lett. 121 193903
[35] Sadrieva Z F and Bogdanov A A 2016 Bound state in the continuum in the one-dimensional photonic crystal slab J. Phys.: Conf. Ser. 741 012122
[36] Zakharov V A and Poddubny A N 2020 Transverse magneto-optical Kerr effect enhanced at the bound states in the continuum Phys. Rev. A 101 043848
[37] Lenzini F et al 2018 Direct characterization of a nonlinear photonic circuit's wave function with laser light Light: Sci. Appl. 7 17143
[38] Luong N, Cheng C-W, Shih M-H and Kuang W 2012 Phase matching for surface plasmon enhanced second harmonic generation in a gold grating slab Appl. Phys. Lett. 100 181107
[39] Sautter J D et al 2019 Tailoring second-harmonic emission from (111)-GaAs nanoantennas Nano Lett. 19 3905–11
[40] Carletti L, Locatelli A, Stepanenko O, Leo G and De Angelis C 2015 Enhanced second-harmonic generation from magnetic resonance in AlGaAs nanoantennas Opt. Express 23 26544–50